Supporting Information

High-Performance Layered Potassium Vanadium Oxide for K-Ion Batteries Enabled by Reduced Long-Range Structural Order

Xiaogang Niu,[a] Jiale Qu,[b] Youran Hong,[c] Leqing Deng,[a] Ruiting Wang,[a] Meiying Feng,[a] Jiangwei Wang,[c] Liang Zeng,[d] Qianfan Zhang, [b]* Lin Guo*[a] and Yujie Zhu* [ae]

[a] School of Chemistry, Beihang University, Beijing 100191, P. R. China

[b] School of Materials Science and Engineering, Beihang University, Beijing 100191, P. R. China

[c] Center of Electron Microscopy and State Key Laboratory of Silicon Materials, School of Materials Science and Engineering, Zhejiang University, Hangzhou 310027, P. R. China

[d] Key Laboratory for Green Chemical Technology of Ministry of Education, School of Chemical Engineering and Technology, Tianjin University, Tianjin 300072, P.R. China

[e] Beijing Advanced Innovation Center for Biomedical Engineering, Beihang University, Beijing 100191, P. R. China

* Corresponding Author: E-mail: qianfan@buaa.edu.cn (Q. Z.), guolin@buaa.edu.cn (L. G.), yujiezhu@buaa.edu.cn (Y. Z.)

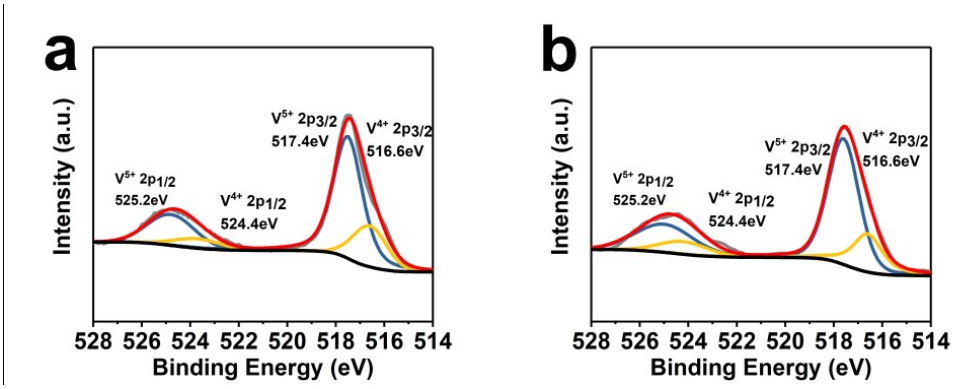

Fig. S1. The high-resolution V2p XPS spectra of a) KVO-H and b) KVO.

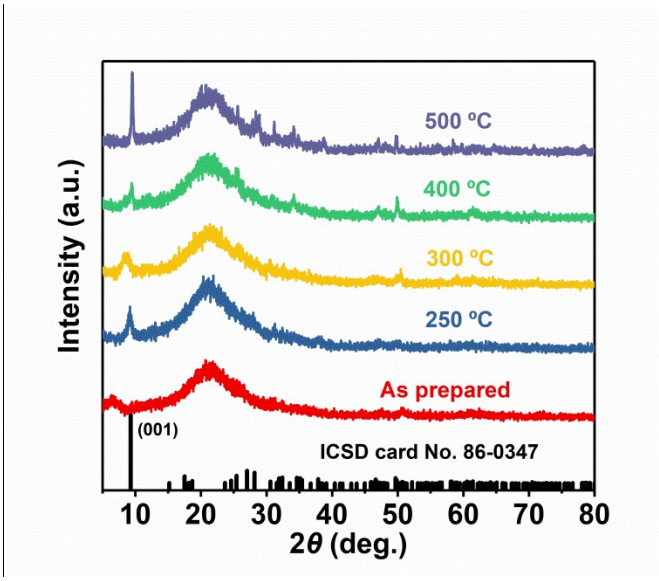

Fig. S2. XRD patterns of the as-prepared KVO-H and the samples annealed at 250, 300, 400, and 500 ˚C, respectively. The standard XRD pattern of monoclinic $K_{0.486}V_2O_5$ (JCPDF No. 86-0347) is also presented.

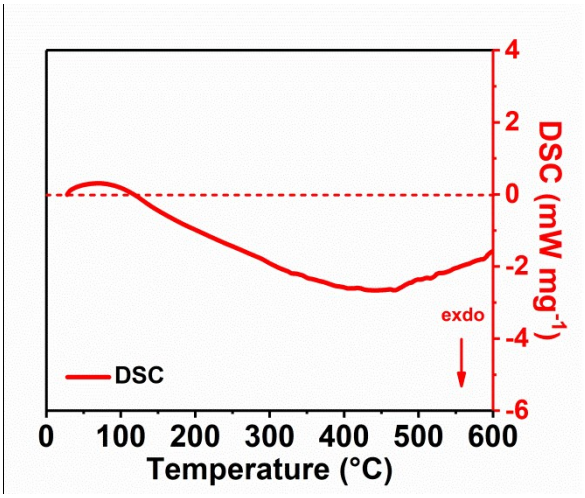

Fig. S3. The DSC profile of KVO-H.

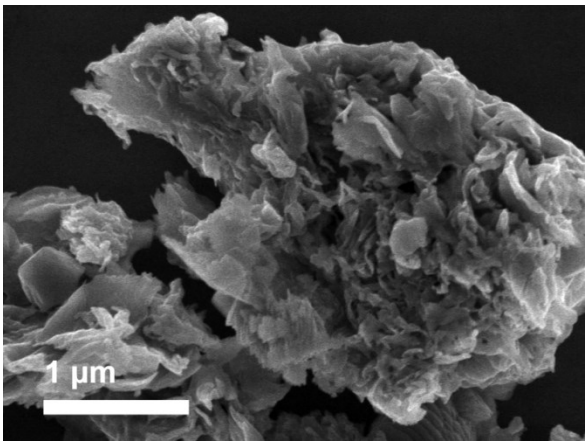

Fig. S4. SEM image of KVO-H.

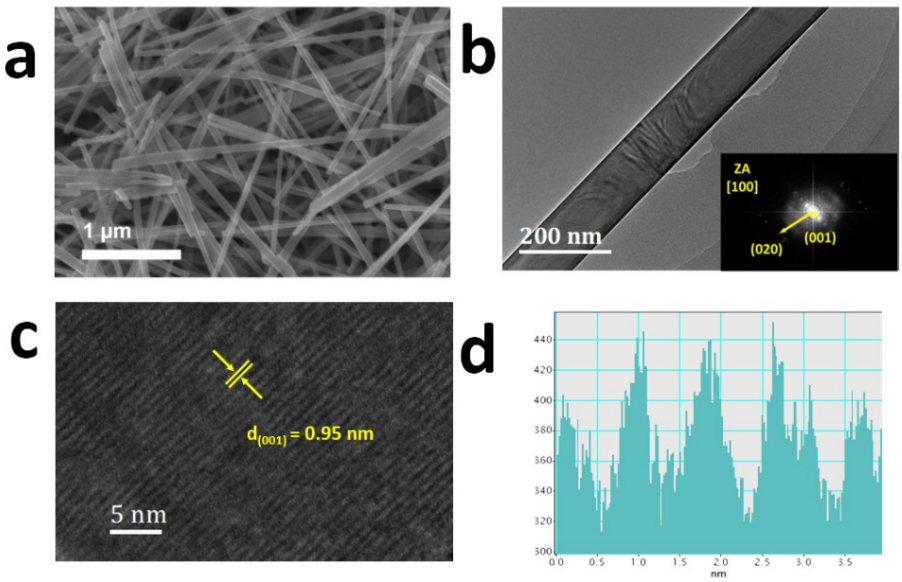

Fig. S5. a) SEM, b) TEM, and c) HRTEM images of KVO. d) Lattice spacing of the (001) plane for KVO measured from the HRTEM image shown in (c).

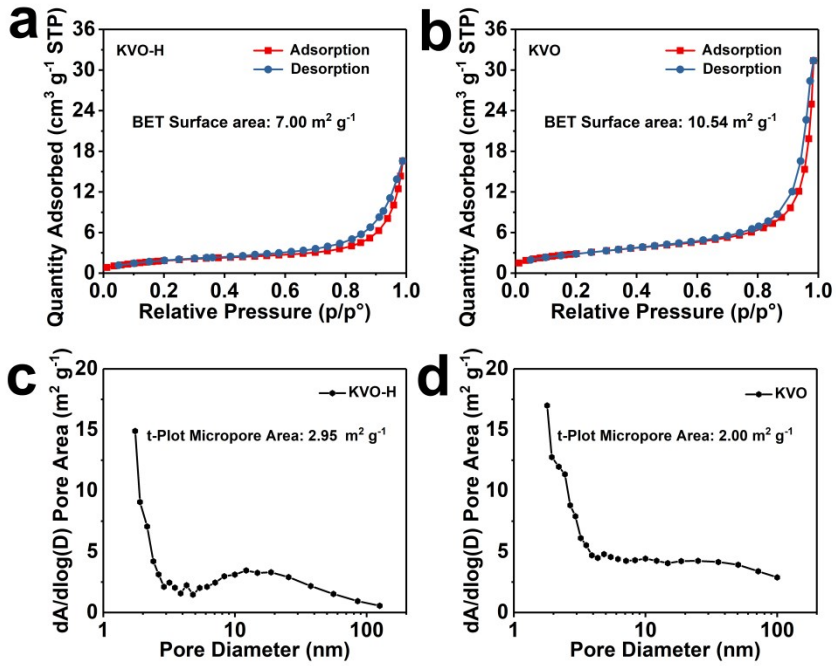

Fig. S6. N_2 adsorption−desorption isotherms and the Brunauer−Emmett−Teller (BET) surface areas of a) KVO-H and b) KVO. Barrett−Joyner−Halenda (BJH) pore areas of (c) KVO-H and (d) KVO.

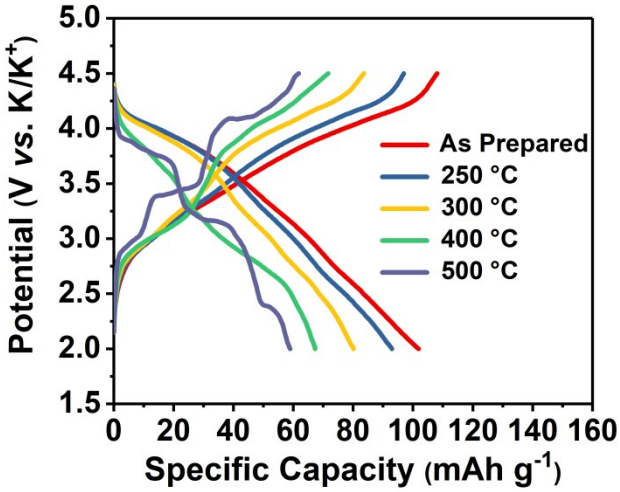

Fig. S7. Charge−discharge curves of KVO-H and the samples annealed at 250, 300, 400, and 500 ˚C, respectively. The specific current 20 mA g^{-1} was used for all the tests.

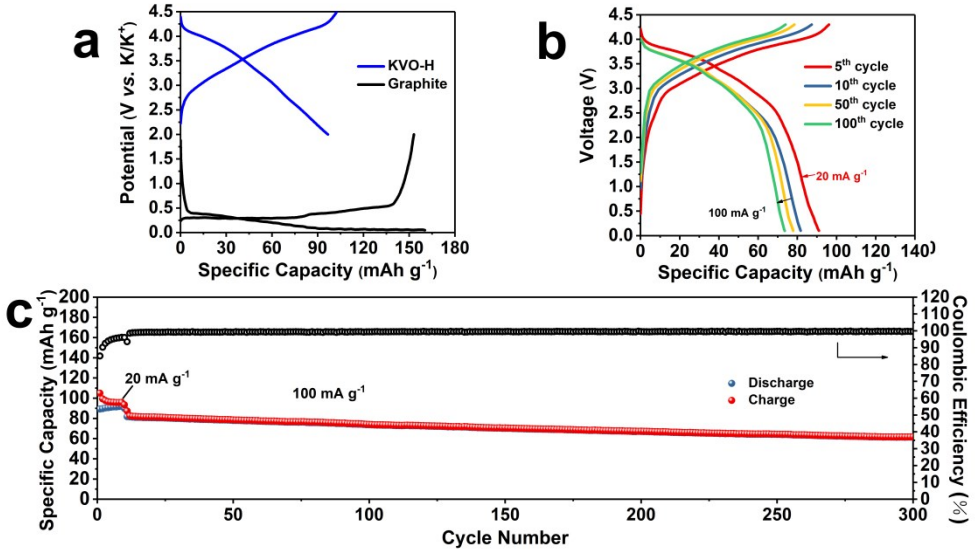

Fig. S8. Electrochemical performance of the full cell. a) Charge–discharge curves of KVO-H and commercial graphite at 20 mA g^{-1}. b) Charge–discharge curves of the full cell at 20 and 100 mA g^{-1}. c) Cycling performance of the full cell at 100 mA g^{-1} with the initial 11 cycles tested at 20 mA g^{-1}.

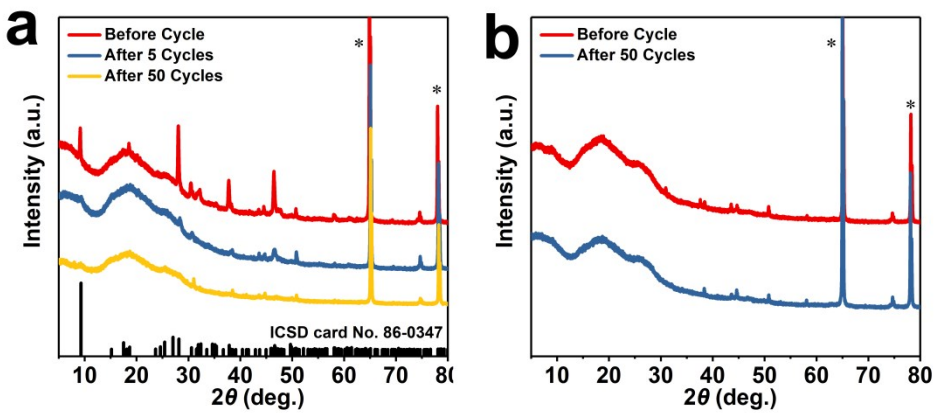

Fig. S9. *Ex-situ* XRD results of (a) the KVO electrode and (b) the KVO-H electrode before and after 50 cycles. The baselines of all XRD results are fixed corresponding to the diffraction signals of the Al current collector at 2θ of 65.1° and 78.2°, which are marked with asterisk.

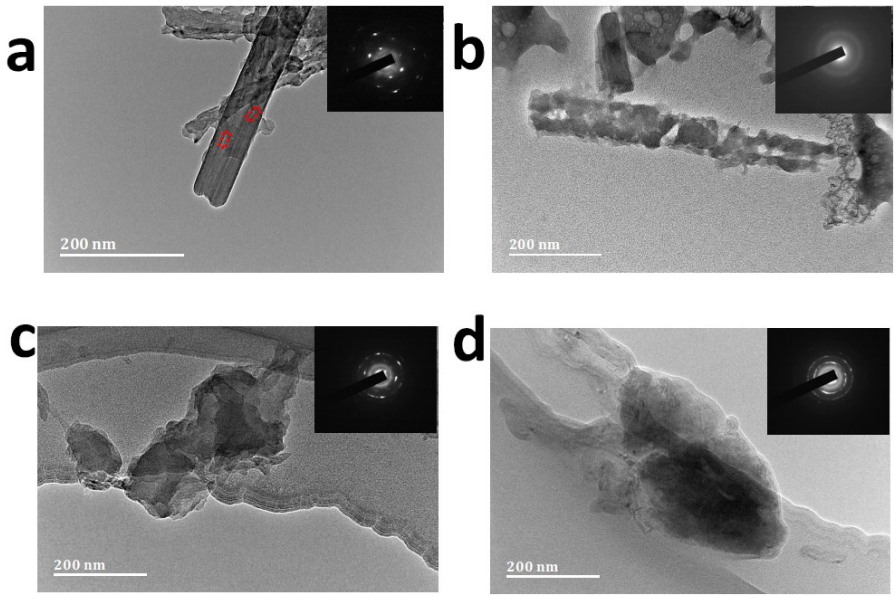

Fig. S10. *Ex-situ* TEM characterization of a, b) KVO and c, d) KVO-H after 1 cycle and 10 cycles, respectively. The insets are the corresponding SAED patterns. The fractures in Fig. S10a are marked by the red dashed squares.

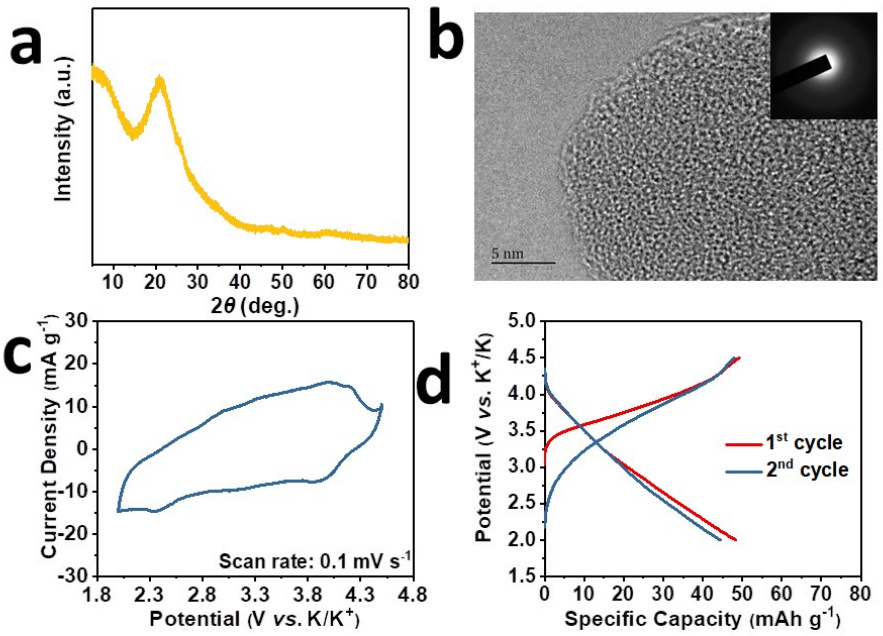

Fig. S11. Characterization of the amorphous $K_{0.5}V_2O_5$. a) XRD pattern, b) HRTEM image and the corresponding SAED image, c) CV profile performed at 0.1 mV s^{-1}, d) charge−discharge curves at the specific current of 20 mA g^{-1}.

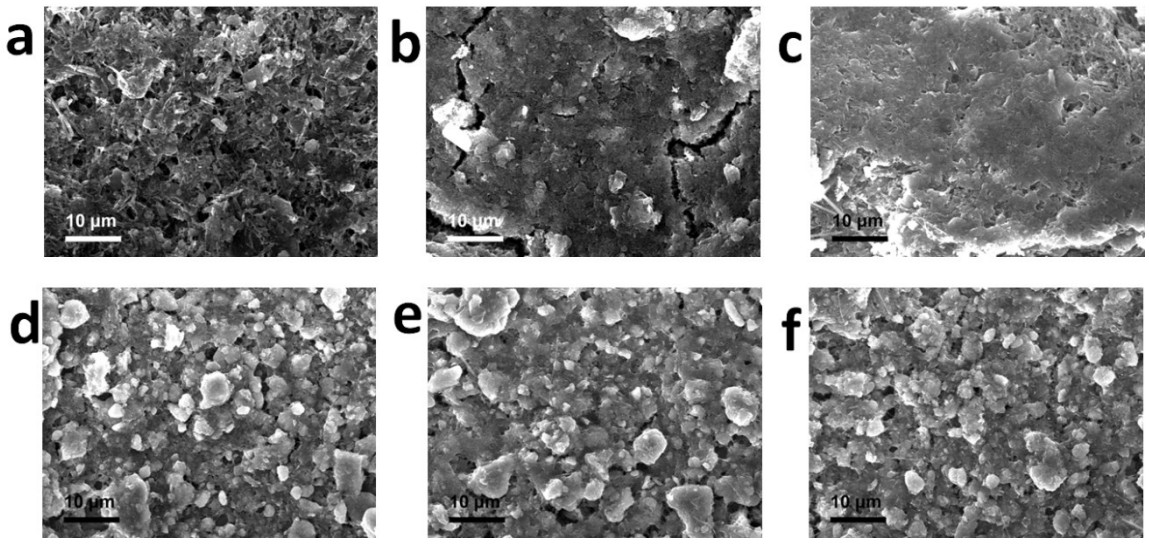

Fig. S12. *Ex-situ* SEM characterization of the KVO electrode: a) before charge-discharge, b) after 1 charge-discharge cycle, and c) after 50 charge-discharge cycles, respectively; *Ex-situ* SEM characterization of the KVO-H electrode: c) before charge-discharge, d) after 1 charge-discharge cycle, and e) after 50 charge-discharge cycles, respectively.

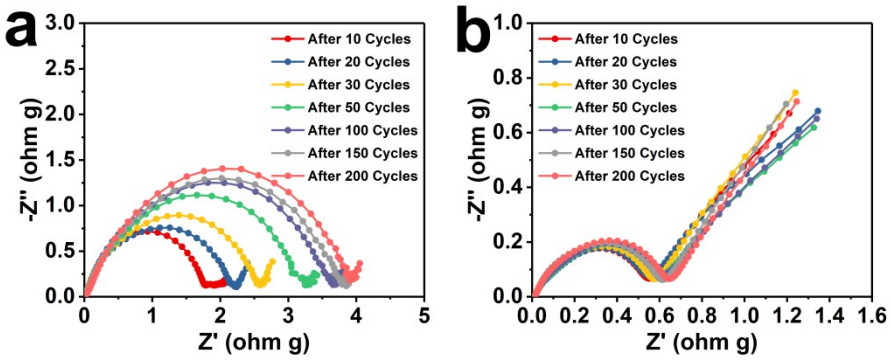

Fig. S13. Nyquist plots of a) the KVO and b) KVO-H electrodes after cycling. All EIS tests were performed at the fully charged state (4.5 V *vs.* K^+/K).

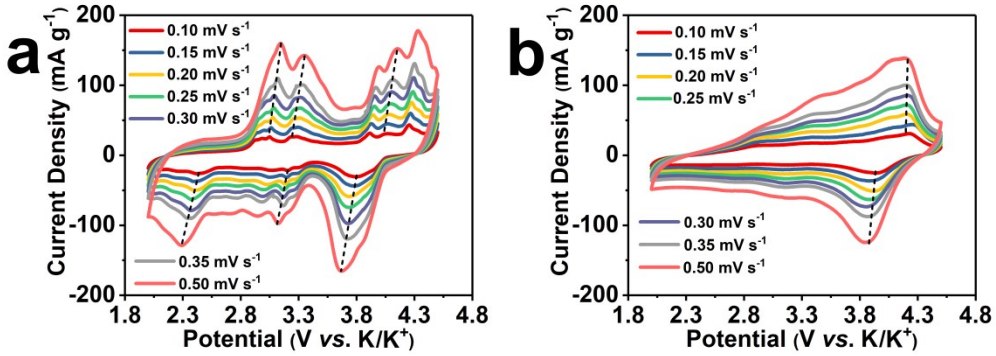

Fig. S14. CV profiles of a) the KVO and b) KVO-H electrodes at different scan rates. The dashed lines in the plots are used as a guide for eyes to show the variations of the current peaks with scan rates.

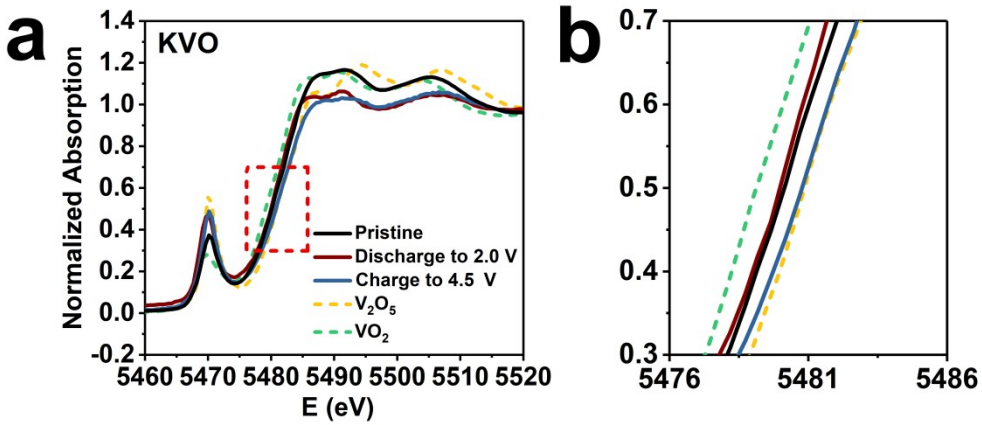

Fig. S15. a) V K-edge XANES spectra for KVO at the fully charged and discharged states. b) The enlarged areas marked by the red dashed square in (a).

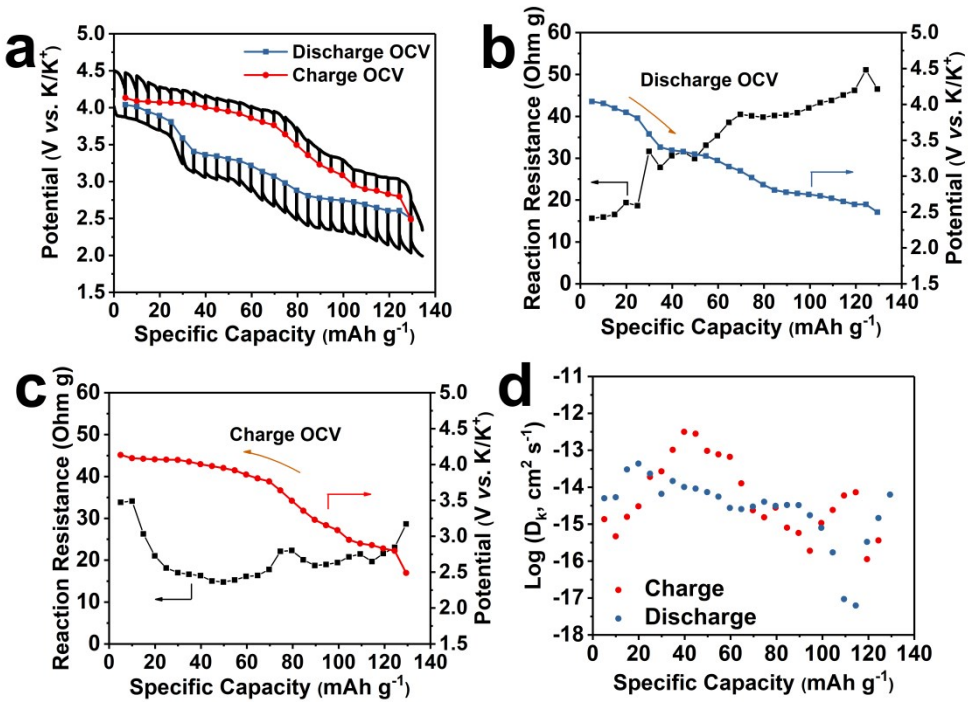

Fig. S16. a) Quasi-equilibrium potential and transient potential profiles *vs.* specific capacity for K-ions intercalation/deintercalation in the KVO obtained from GITT. b) Reaction resistance for K-ions intercalation into the KVO. c) Reaction resistance for K-ion deintercalation from the KVO. d) The calculated apparent chemical diffusion coefficient of potassium (D_K) in the KVO *vs.* specific capacity.

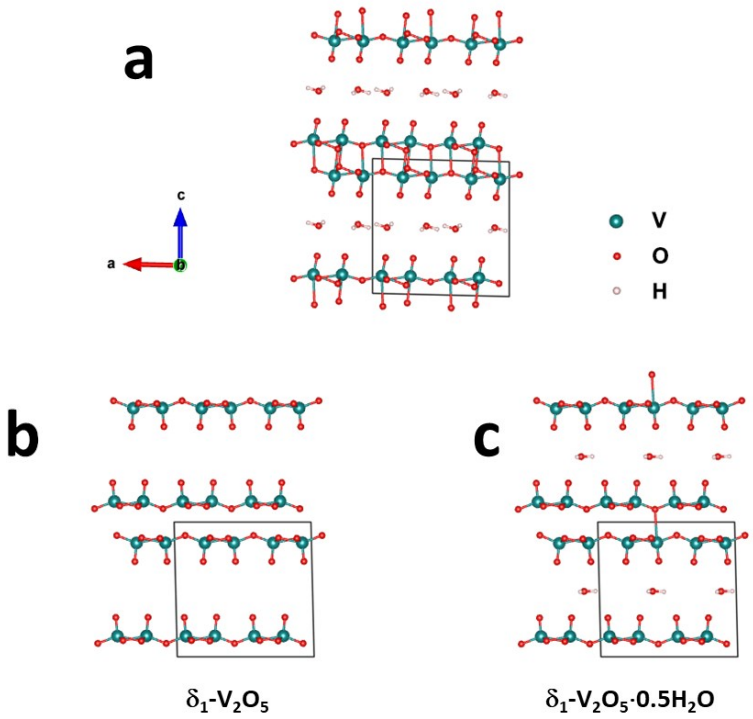

Fig. S17. Structures of a) δ-V_2O_5·H_2O, b) δ_1-V_2O_5, and c) δ_1-V_2O_5·0.5H_2O.

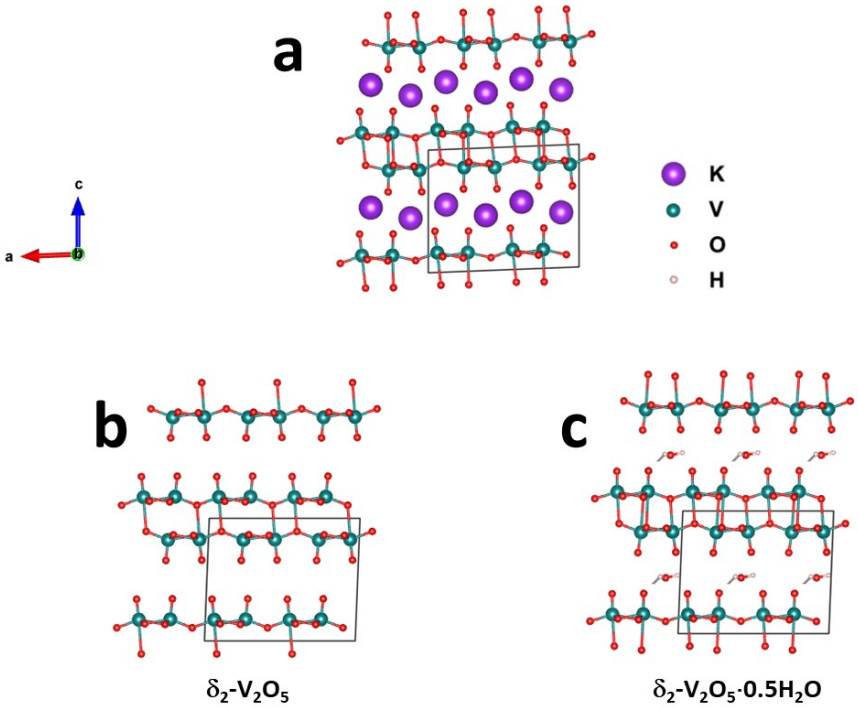

Fig. S18. Structures of a) δ-$K_{0.5}V_2O_5$, b) δ_2-V_2O_5, and c) δ_2-$V_2O_5 \cdot 0.5H_2O$.

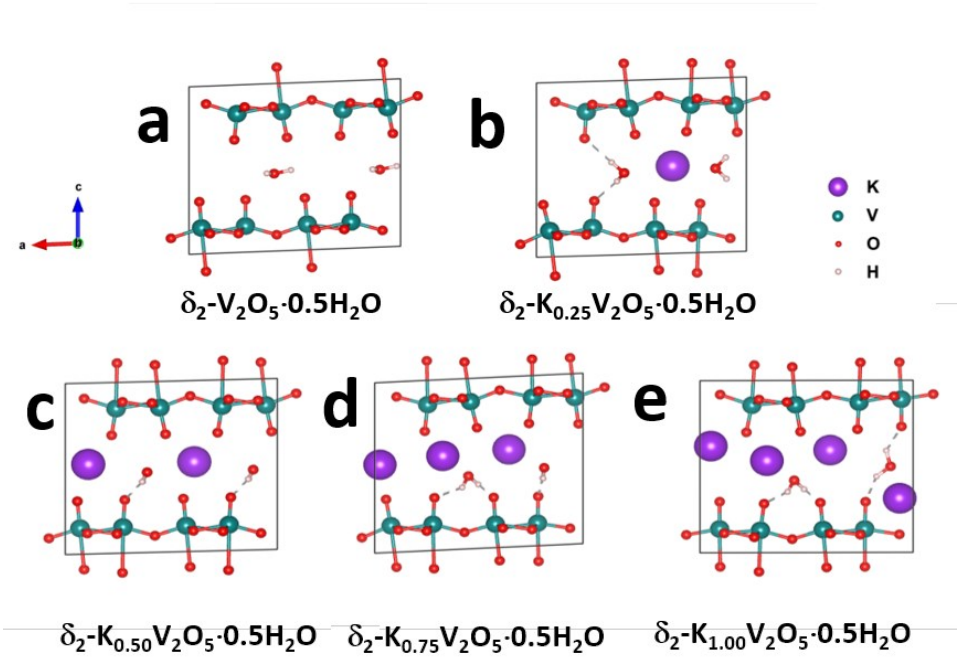

Fig. S19. Structures of a) δ_2-V_2O_5·0.5H_2O, b) δ_2-$K_{0.25}V_2O_5$·0.5H_2O, c) δ_2-$K_{0.50}V_2O_5$·0.5H_2O, d) δ_2-$K_{0.75}V_2O_5$·0.5H_2O, and e) δ_2-$K_{1.00}V_2O_5$·0.5H_2O.

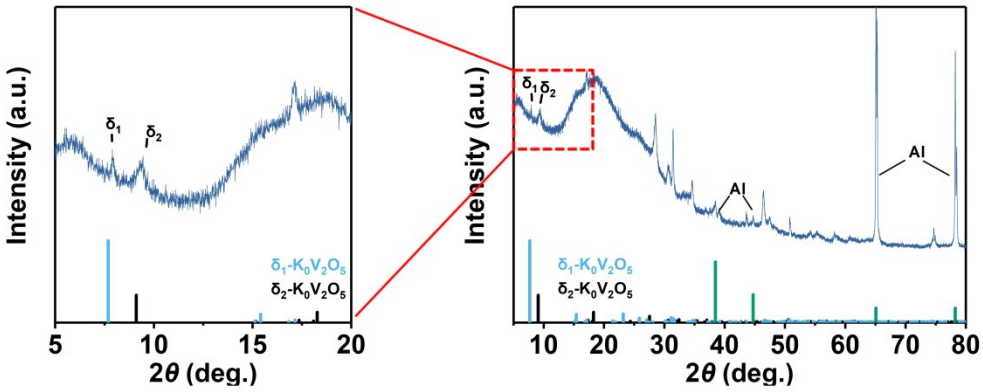

Fig. S20. Comparison of the XRD result of the KVO electrode at the fully charged state after the first charge process with the expected diffraction response of δ_1-V_2O_5 and δ_2-V_2O_5 obtained from the DFT calculations. The diffraction signals of Al current collector are also marked in the plot.

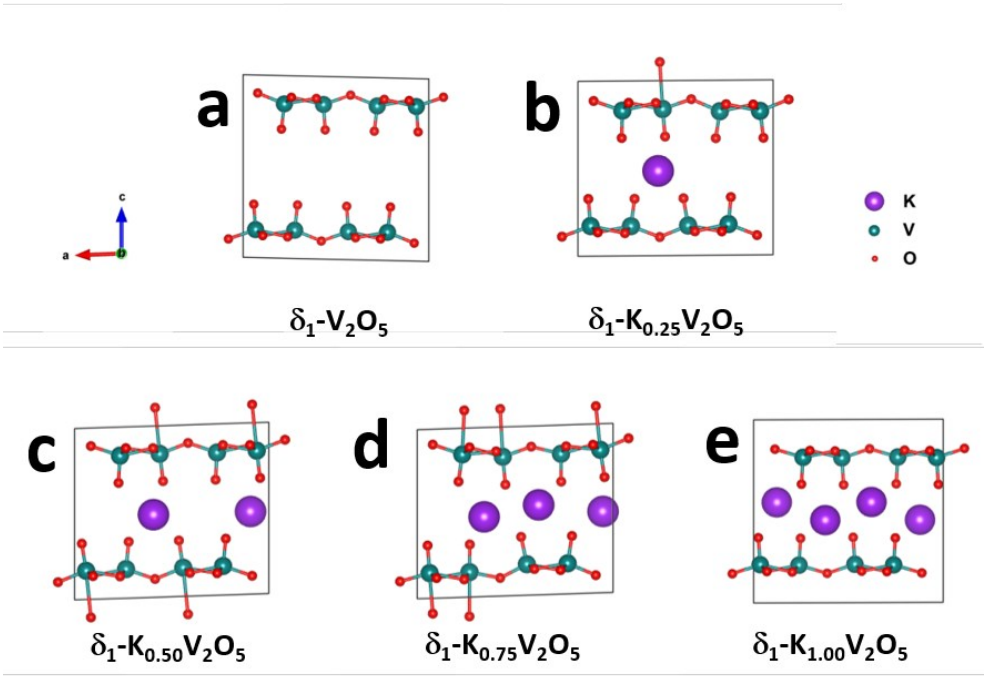

Fig. S21. Structures of a) δ_1-V_2O_5, b) δ_1-$K_{0.25}V_2O_5$, c) δ_1-$K_{0.50}V_2O_5$, d) δ_1-$K_{0.75}V_2O_5$, and e) δ_1-$K_{1.00}V_2O_5$.

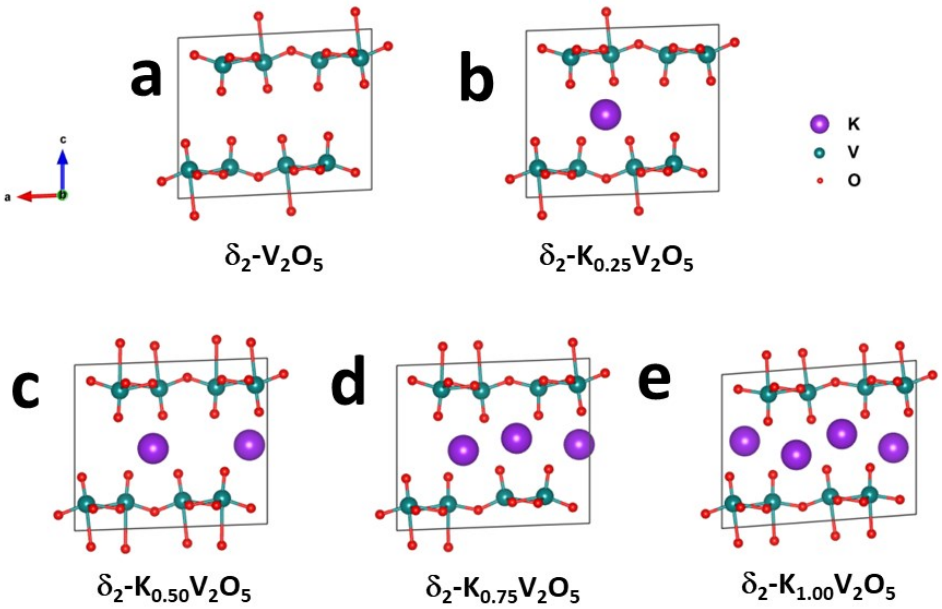

Fig. S22. Structures of a) δ_2-V_2O_5, b) δ_2-$K_{0.25}V_2O_5$, c) δ_2-$K_{0.50}V_2O_5$, d) δ_2-$K_{0.75}V_2O_5$, and e) δ_2-$K_{1.00}V_2O_5$.

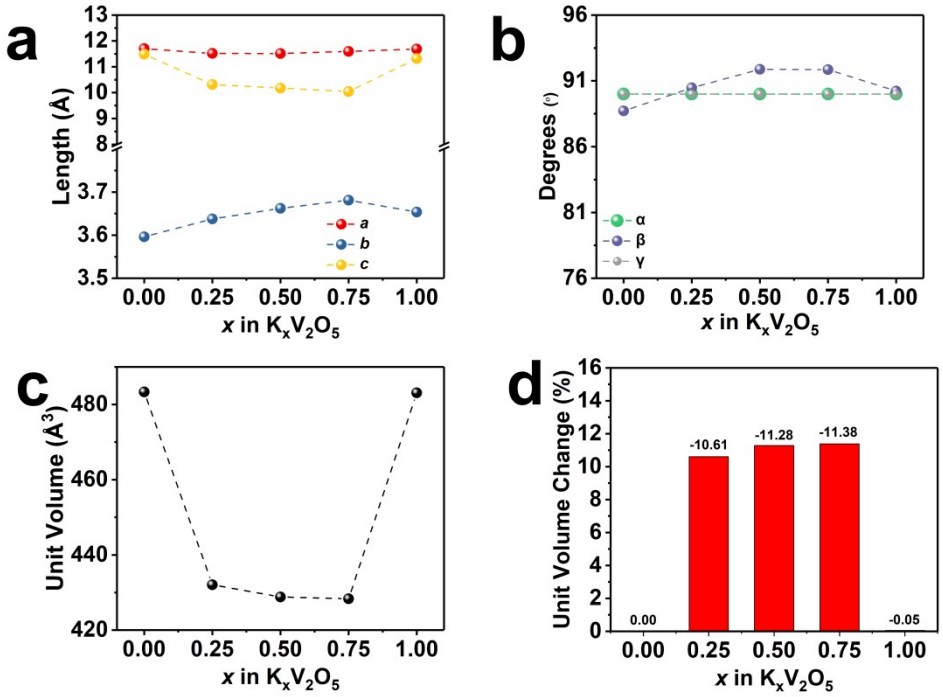

Fig. S23. The calculated (a and b) lattice parameters and (c) unit cell volumes of δ_1-$K_xV_2O_5$ ($0 \leq x \leq 1$) at various K-ion contents. (d) The difference of the unit cell volume between δ_1-$K_xV_2O_5$ ($0 \leq x \leq 1$) and δ_1-V_2O_5.

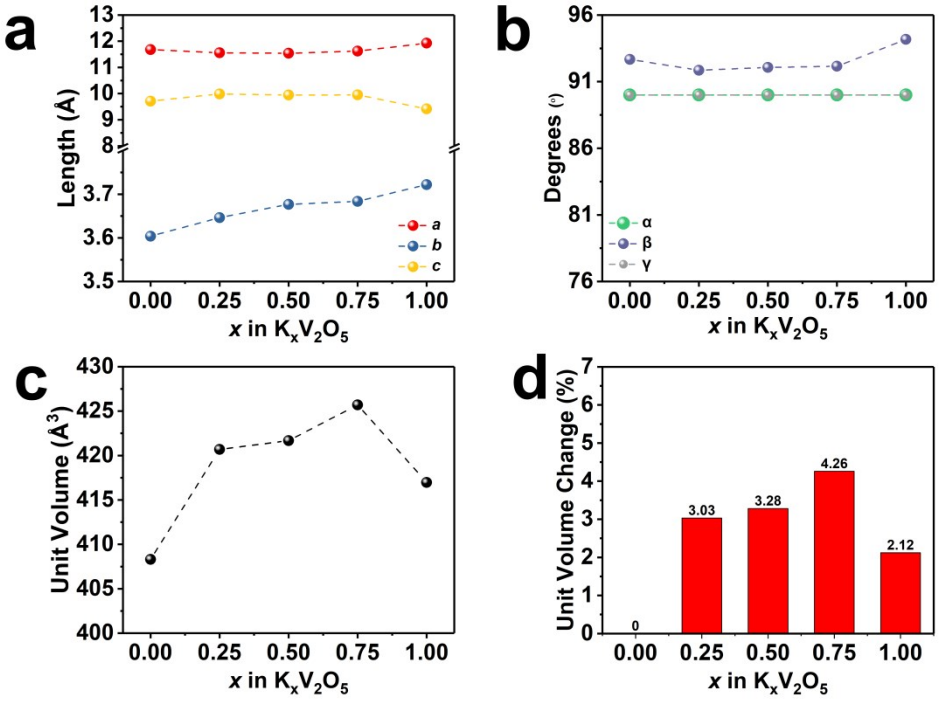

Fig. S24. The calculated (a and b) lattice parameters and (c) unit cell volumes of δ_2-$K_xV_2O_5$ ($0 \leq x \leq 1$) at various K-ion contents. (d) The difference of the unit cell volume between δ_2-$K_xV_2O_5$ ($0 \leq x \leq 1$) and δ_2-V_2O_5.

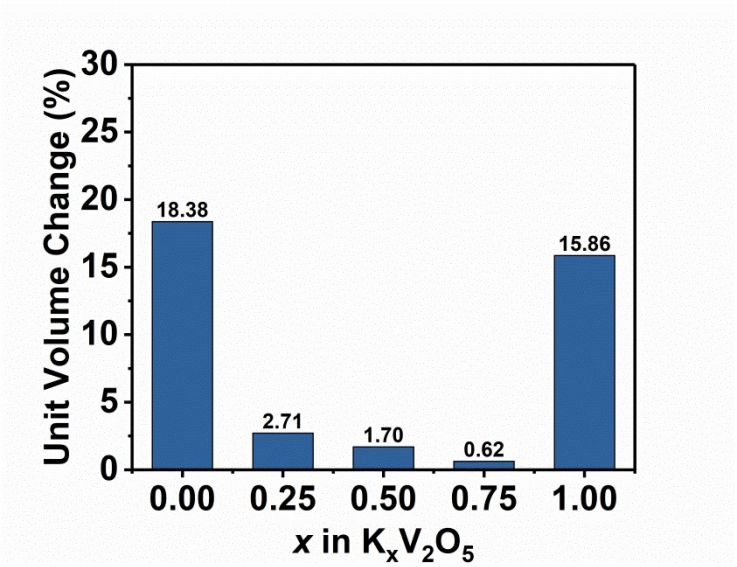

Fig. S25. The unit cell volume difference between δ_1-$K_xV_2O_5$ and δ_2-$K_xV_2O_5$ ($0 \leq x \leq 1$) in comparison with the unit cell volume of δ_2-$K_xV_2O_5$ ($0 \leq x \leq 1$).